A Computational Tool for Time-Series Prediction of Mining-Induced Subsidence Based on Time-Effect Function and Geodetic Monitoring Data

Nguyen Quoc Long[1(✉)] , Xuan-Nam Bui[2] , Luyen Khac Bui[3] ,
Khoa Dat Vu Huynh[4], Canh Van Le[1] , Michał Buczek[5] ,
and Thang Phi Nguyen[1]

[1] Department of Mine Surveying,
Hanoi University of Mining and Geology, Hanoi, Vietnam
nguyenquoclong@humg.edu.vn
[2] Department of Surface Mining,
Hanoi University of Mining and Geology, Hanoi, Vietnam
[3] Department of Geodesy,
Hanoi University of Mining and Geology, Hanoi, Vietnam
[4] Norwegian Geotechnical Institute (NGI), Oslo, Norway
[5] Department of Engineering Surveying and Civil Engineering,
AGH University of Science and Technology, Kraków, Poland

Abstract. Underground mining-induced land subsidence may cause serious damage to engineering structures (e.g., buildings or roads) therefore, it is necessary to predict the subsidence with the highest possible accuracy. This paper proposes a new method for estimating preliminary values of the parameters to the modified Knothe time function, resulting in an improved capability of predicting land subsidence. A computational tool incorporating the proposed method has been developed to practically and numerically facilitate the time-series prediction of mining subsidence. A case study at the Mong Duong colliery at Quang Ninh province in Vietnam was considered and back-analyzed to validate the capability and accuracy of the tool. The accuracy of the subsidence prediction was evaluated using Root Mean Square Errors (*RMSE*), Mean Absolute Errors (*MAE*), and the Correlation coefficient (*r*). The result showed that the proposed method predicted reasonably well both the calibrating dataset (*RMSE* = 15 mm, *MAE* = 13 mm, *r* = 0.996) and the validating dataset (*RMSE* = 44 mm, *MAE* = 37 mm, *r* = 0.857). Based on the comparison results, it is concluded that the developed tool incorporating the proposed method is suitable for predicting underground mining-induced land subsidence.

Keywords: Computational tool · Time-series prediction · Modified knothe time function · Underground mining · Geodetic monitoring

1 Introduction

The rapid growths in the world's population and economy have resulted in continuous increase in energy and mineral consumption. To meet this high demand for minerals, mining activities have continuously and rapidly expanded over time, all over the world. Underground coal mining can cause serious damages, as a result of mining-induced land subsidence, to engineering structures such as buildings, roads, railways, and drainage systems [1–3]. It is important to note that mining-induced land subsidence can occur not only during active mining but also several decades after the completion of active mining. In Vietnam, damage caused by mine surface deformation is commonly observed and occurs in most of all underground mining areas, especially at the Quang Ninh coal basin [4]. For example, in 1991 mining-induced subsidence caused huge damage to the road at the Deo Nai mine [5]. In 2000, a subsidence observed at the Mao Khe coal mine caused serious damage for the fan station [4]. Several residential houses were heavily damaged and the 110 kV electricity line was destroyed because of a subsidence at the Mong Duong colliery [6, 7]. It is concluded that one of the main reasons of causing the above land subsidence phenomena in Vietnam was the lack of practical and sophisticated methods for accurately predicting mining-induced land subsidence.

Many methods have been developed and continuously improved to better predict and estimate land subsidence due to mining activities [1, 8, 9]. According to Bahuguna, et al. [10], subsidence prediction methods can be basically classified into three categories: empirical techniques, influence function and theoretical modelling. Among them, the Knothe time function (KTF) is considered to be the most effective and widely used [11, 12]. The major advantage of the KTF method is that it can describe the process of surface subsidence in time through a set of differential mathematical equations [13, 14]. By using the KTF method, land subsidence over time due to underground mining activity can be simply predicted through a subsidence curve. However, land subsidence is generally a complex and nonlinear process so that the application of the original KTF method is not able to correctly capture the whole process of surface subsidence. Wang [15] reported that the prediction accuracy of the KTF models could be low in many cases. Therefore, some modifications of KTF have been proposed [16–18], i.e. a modified function adding a constant parameter to the KTF [19]. Although many recent modified KTF models have made it possible to accurately predict land subsidence over time, it is still difficult and time-consuming to properly determine the function parameters due to the fact that these parameters heavily depend on the estimation of their preliminary values [19]. Therefore, research works are still needed to further improve the prediction accuracy of mining-induced land subsidence.

This research addresses the aforementioned limitation by proposing a new method for estimating the preliminary parameter values of the modified KTF model proposed by Chinh [19], leading to an improved capability of predicting land-surface subsidence. The proposed method was further used to develop a computational tool for time-series prediction of mining subsidence. It is noted that the computational tool was developed using Visual C.net programing language. A case study of the Mong Duong colliery at Quang Ninh province in Vietnam was considered to validate both the current model and the computational tool. The geodetic time-series data of mining subsidence

measured from 2013 to 2015 with 12 epochs were used as input to the modified KTF model. The subsidence prediction accuracy was assessed using Root Mean Square Error (*RMSE*), Mean Absolute Error (*MAE*), and the Correlation coefficient (*r*).

2   Methodology

2.1   Knothe Time Function and Its Modified Version

According to Knothe [13, 14], the relationship between a time parameter and land subsidence can be established using the following equation:

$$\frac{d\eta(t)}{dt} = b[\eta_{max} - \eta(t)] \tag{1}$$

where b is a parameter describing the influence of geological and mining conditions on the subsidence progress with time; η_{max} and $\eta_{(t)}$ are the final subsidence and the subsidence at the time t, respectively.

By integrating Eq. 1 with respect to t, the KTF model for surface dynamic subsidence could be written as below:

$$\eta^p(t_i) = \eta_{max}.\left[1 - e^{-bt_i}\right] \tag{2}$$

It is observed from Eq. 2 that there is only one parameter b which plays a significant role in predicting surface subsidence. This limitation could result in low prediction accuracy when using the KTF model in many cases [15]. To improve the prediction, Chinh [19] proposed a modified KTF model described as follows:

$$\eta^p(t_i) = \eta_{max}\left[1 - e^{-b(t_i)^c}\right] \tag{3}$$

where $\eta^p(t_i)$ is the predicted subsidence of the ith epoch; c is the fitting parameter.

Literature review indicates that the preliminary value of c equal to 2 is commonly assumed in various works [19]. The uncertainty in defining the fitting parameter c may result in large errors in some complex land subsidence. In some cases, it is even impossible to find c in a given dataset. Thus, the approach used for estimating the preliminary c-value needs to be improved in order to better determine the parameter c.

2.2   Method for Determination of Preliminary Parameters

From Eq. 3, the relation between $\eta^p(t_i)$ and the measured value $\eta(t_i)$ can be derived as:

$$\eta^p(t_i) = \eta(t_i) + V_{\eta(t_i)} \tag{4}$$

where $V_{\eta(t_i)}$ is residual value at the time t_i. The model parameters η_{max}, b, c are determined based on the least-squares principle using the following equations:

$$\begin{cases} \eta_{max} = \eta_{max}^0 + \delta\eta_{max} \\ \quad b = b^0 + \delta b \\ \quad c = c^0 + \delta c \end{cases} \tag{5}$$

where η_{max}^0, b^0, c^0 are the preliminary values of the modified KTF; $\delta\eta_{max}, \delta b, \delta c$ are the residual ones.

Based on Eq. 4 and the system of Eq. 5, the residual equation can be rewritten as follows:

$$V_{\eta(t_i)} = \eta^P(t_i)\left(\eta_{max}^0 + \delta\eta_{max}, b^0 + \delta b c^0 + \delta c\right) - \eta(t_i) \tag{6}$$

To estimate preliminary values for η_{max}^0, b^0, c^0, the following steps are proposed: Rewriting Eq. 3 as follows:

$$1 - \frac{\eta(t_i)}{\eta_{max}^0} = e^{-b^0(t_i)^{c^0}} \tag{7}$$

By taking the natural logarithm of the both sides of Eq. 7, the modified KTF model will become:

$$\ln\left[1 - \frac{\eta(t_i)}{\eta_{max}^0}\right] = -b^0(t_i)^{c^0} = > (t_i)^{c^0} = \frac{\ln\left[1 - \frac{\eta(t_i)}{\eta_{max}^0}\right]}{-b^0} \tag{8}$$

At the $(i+1)^{th}$ epoch, Eq. 8 is formed as:

$$(t_{i+1})^{c^0} = \frac{\ln\left[1 - \frac{\eta(t_{i+1})}{\eta_{max}^0}\right]}{-b^0} \tag{9}$$

Dividing Eqs. 8 and 9 gives the following equation for estimating preliminary parameter c^0:

$$c^0 = \log_{\frac{t_i}{t_{i+1}}}\left[\frac{\ln\left[1 - \frac{\eta(t_i)}{\eta_{max}^0}\right]}{\ln\left[1 - \frac{\eta(t_{i+1})}{\eta_{max}^0}\right]}\right] \tag{10}$$

The value c^0 from Eq. 10 is substituted into Eq. (8), then b^0 can be determined as follows:

$$b^0 = -\frac{\ln\left[1 - \frac{\eta(t_i)}{\eta_{max}^0}\right]}{(t_i)^{c^0}} \tag{11}$$

2.3 Computation of Modified KTF Parameters

If the preliminary parameters are estimated sufficiently close to their desired values then the residuals are small. In this case, the residual value $V_{\eta(t_i)}$ in Eq. 4 can be approximated by a Taylor series expansion, retaining only the first order terms of $\partial_{\eta_{max}}$, δb, δc as follows:

$$
\begin{aligned}
V_{\eta(t_i)} &= \eta^p(t_i)\left(\eta_{max}^0, b^0, c^0\right) + \left(\frac{\partial \eta^p(t_i)}{\partial_{\eta_{max}}}\right)_0 \delta_{\eta_{max}} + \left(\frac{\partial \eta^p(t_i)}{\partial_b}\right)_0 \delta_b \\
&\quad + \left(\frac{\partial \eta^p(t_i)}{\partial_c}\right)_0 \delta_c - \eta(t_i)
\end{aligned}
\tag{12}
$$

where $\frac{\partial \eta^p(t_i)}{\partial_{\eta_{max}}} = 1 - e^{-b^0(t_i)^{c^0}}$; $\frac{\partial \eta^p(t_i)}{\partial_b} = \eta_{max}(t_i)^{c^0} e^{-b^0(t_i)^{c^0}}$;

and $\frac{\partial \eta^p(t_i)}{\partial_c} = \eta_{max} b^0 . e^{-b^0(t_i)^{c^0}}(t_i)^{c^0} \ln(t_i)$

The residual between the predicted values and their corresponding measured values is expressed as follows:

$$
\ell_i = \eta^p(t_i)\left(\eta_{max}^0, b^0, c^0\right) - \eta(t_i)
\tag{13}
$$

Finally, the observation equation is derived as:

$$
V_{\eta(t_i)} = \left(\frac{\partial \eta^p(t_i)}{\partial_{\eta_{max}}}\right)_0 \delta_{\eta_{max}} + \left(\frac{\partial \eta^p(t_i)}{\partial_b}\right)_0 \delta_b + \left(\frac{\partial \eta^p(t_i)}{\partial_c}\right)_0 \delta_c + \ell_i
\tag{14}
$$

The coefficients of Eq. 14 are symbolized as $\left(\frac{\partial \eta^p(t_i)}{\partial_{\eta_{max}, b, c}}\right)_0 = a_{ij}$, with $i = 1 \div n$ and $j = 1, 2, 3$, corresponding to the unknowns $\partial_{\eta_{max}}$, δ_b, δ_c. By doing so, a system of linear equations in Eq. 14 can be represented in matrix form as follows:

$$
V = A.X + L
\tag{15}
$$

where A is the design matrix, V is the vector of discrepancies, L is the vector of observations, and X is the vector of unknowns.

$$
A = \begin{bmatrix} a_{1,1} & a_{1,2} & a_{1,3} \\ a_{2,1} & a_{2,2} & a_{2,3} \\ \cdots & \cdots & \cdots \\ a_{n,1} & a_{n,2} & a_{n,3} \end{bmatrix}; \; V = \begin{bmatrix} V_1 \\ V_2 \\ \cdots \\ V_n \end{bmatrix}; \; L = \begin{bmatrix} \ell_1 \\ \ell_2 \\ \cdots \\ \ell_n \end{bmatrix}; \; X = \begin{bmatrix} \partial_{\eta_{max}} \\ \delta_b \\ \delta_c \end{bmatrix}.
\tag{16}
$$

The following normal equation can be derived from a set of different observation equations:

$$
\left(A^T A\right)X + \left(A^T L\right) = 0
\tag{17}
$$

$$
X = -\left(A^T A\right)^{-1} A^T L
\tag{18}
$$

Considering these derived X values, parameters η_{max}, b, c of the prediction model can be firstly determined by Eq. 5, and then Eq. 3 is used to calculate the subsidence value of the ith epoch.

2.4   Accuracy Assessment

Accuracy of the current prediction model is assessed by comparing the predicted result with the measured data in terms of Root Mean Square Error (*RMSE*), mean absolute error (*MAE*) and correlation coefficient (*r*). The lower *RMSE* and *MAE* together with the higher *r* indicate the more accurate prediction of the model. More specifically, the following equations are used:

$$RMSE = \sqrt{\frac{1}{\text{n}} \sum_{i=1}^{n} \left[\eta^p(t_i) - \eta(t_i) \right]^2} \tag{19}$$

$$MAE = \frac{1}{n} \sum_{i=1}^{n} |\eta(t_i) - \eta^p(t_i)| \tag{20}$$

$$r = \frac{\sum_{i=1}^{n} (\eta(t_i) - \bar{\eta})(\eta^p(t_i) - \overline{\eta^p})}{\sqrt{\sum_{i=1}^{n} (\eta(t_i) - \bar{\eta})^2 * \sum_{i=1}^{n} (\eta^p(t_i) - \overline{\eta^p})^2}} \tag{21}$$

where $\eta(t_i)$ and $\eta^p(t_i)$ are the measured and the predicted values at t_i; $\bar{\eta}$ and $\overline{\eta^p}$ are the corresponding medium values of measured and predicted values, respectively.

3   Computational Tool for Time-Series Prediction of Mining Subsidence

Based on the modified KTF method proposed in the Sect. 2, a computational tool for time-series prediction of mining subsidence was developed. It is noted that the tool was programmed in Visual Studio.Net 2013 Ultimate, an object-oriented programming language with Visual Studio DevExpress Universal 15.2.7 library package [20]. The tool can run in different versions of Microsoft Windows including the version 7, 8 and 10 and it is also compatible with both 32- and 64-bit environments.

Figure 1 presents a workflow for the determination of the preliminary parameters (η_{max}^0, b^0, c^0) of the modified KTF method. A workflow for the computation of the corresponding final parameters (η_{max}, b, c) based on the least-squares principle and accuracy assessment (*RMSE*, *MAE* and *r*) is illustrated in Fig. 2.

A Graphic User Interface (GUI) of the computational tool is shown in Fig. 3. Input data could be either entered directly through the GUI or imported from text or excel files. The computed results including the model's parameters and the predicted values, are stored both in txt and csv formats, which make them easier to be shared with and edited by other softwares. Furthermore, measurement data and prediction results can be exported/converted into a graphical file in Drawing Exchange Format (DXF). DXF is a
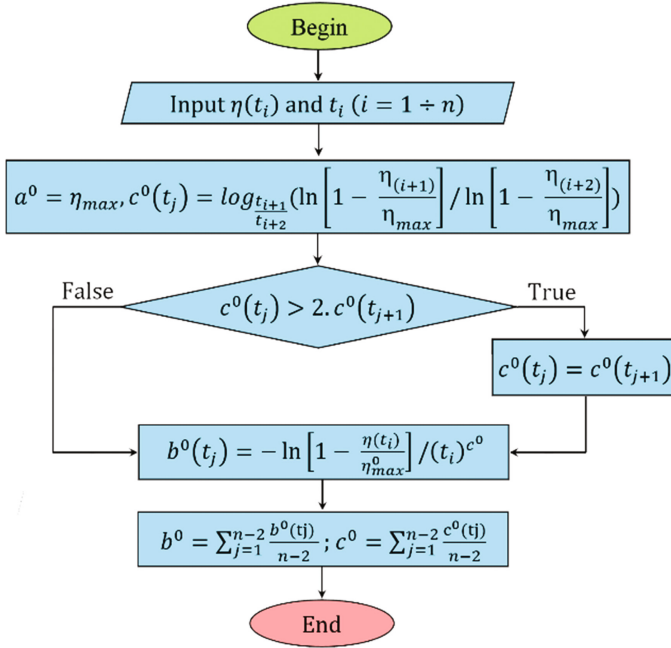
Fig. 1. Workflow used for estimating preliminary parameters of modified KTF

CAD data file format developed by Autodesk for enabling data interoperability between AutoCAD and other programs [21].

4 A Case Study of Mining Subsidence at Mong Duong Colliery, Quang Ninh Province in Vietnam

4.1 Description of the Study Site

Mong Duong colliery, a typical coal mine in Vietnam with more than 35-year operation, is selected as a case study for validating the modified KTF model. This mine is located about 10 km north of Cam Pha city, as shown in Fig. 4. The mine boundary was taken according to the Decision No. 1122/QD-HDQT dated on May 16, 2008, by the Chairman of the Vinacomin's Board of Directors on Approving the master plan for coal mines boundary of the Vietnam National Coal - Mineral Industries Holding Corporation Limited.

From explorations' results, there are in total 22 coal seams in the Mong Duong colliery. To date, the coal is excavated in various seams and multi-layer seams, mainly varying from −100 m to −250 m below the sea level. They consist of seams H10, G9 in the East Wing, G9 in the West Wing, G9 in Vu Mon area, II (11) and K8, etc. There are two shafts including the main shaft and the auxiliary shaft, which were built correspondingly from +18 m and +6.5 m down to −97.5 m.
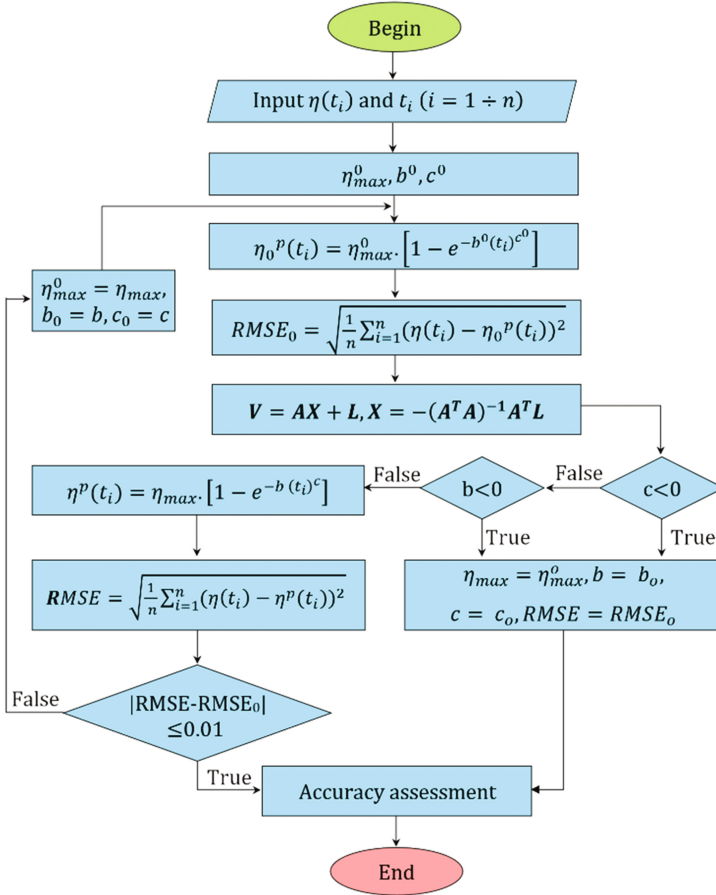
Fig. 2. Workflow used for the computing final parameters of modified KTF

Underground mining activity in the Mong Duong colliery has resulted in various subsidence problems that caused several damages to residential areas, the main shaft, the wind turbine station, the 110/35/6 kV substation and office buildings on the mine surface.

4.2   Data Collection and Processing

To assess and forecast potential land subsidence due to the underground mining at the Mong Duong colliery, a monitoring network has been established in the G9 BMD seam, where the Face No.2 was mined. The G9 BMD seam has an average thickness of 2.5 m with an average slope angle of 35°. The Face No.2 was commenced in the second quarter 2013 and finished in second quarter 2014. The panel was prepared along the seam strike and retreated, cutting coal by blasting and supporting the roof using hydraulic props (Fig. 5).

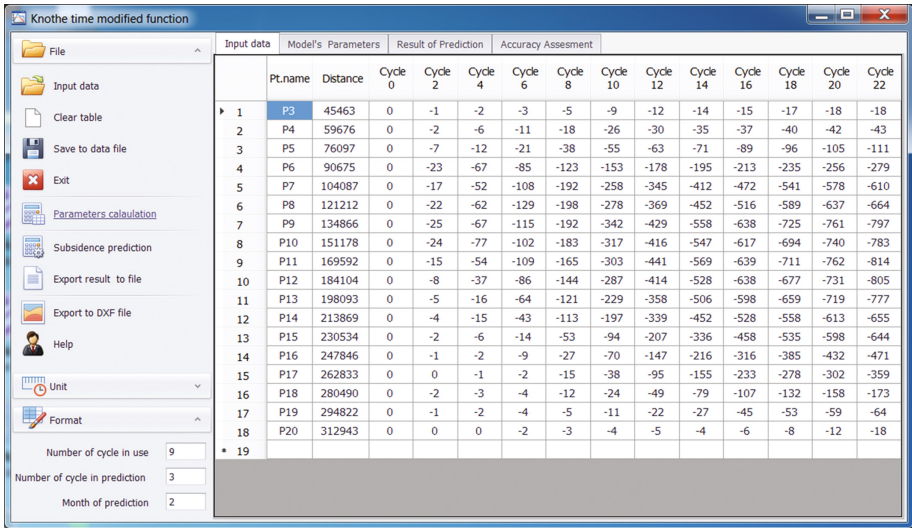| Pt.name	Distance	Cycle 0	Cycle 2	Cycle 4	Cycle 6	Cycle 8	Cycle 10	Cycle 12	Cycle 14	Cycle 16	Cycle 18	Cycle 20	Cycle 22
P3	45463	0	-1	-2	-3	-5	-9	-12	-14	-15	-17	-18	-18
P4	59676	0	-2	-6	-11	-18	-26	-30	-35	-37	-40	-42	-43
P5	76097	0	-7	-12	-21	-38	-55	-63	-71	-89	-96	-105	-111
P6	90675	0	-23	-67	-85	-123	-153	-178	-195	-213	-235	-256	-279
P7	104087	0	-17	-52	-108	-192	-258	-345	-412	-472	-541	-578	-610
P8	121212	0	-22	-62	-129	-198	-278	-369	-452	-516	-589	-637	-664
P9	134866	0	-25	-67	-115	-192	-342	-429	-558	-638	-725	-761	-797
P10	151178	0	-24	-77	-102	-183	-317	-416	-547	-617	-694	-740	-783
P11	169592	0	-15	-54	-109	-165	-303	-441	-569	-639	-711	-762	-814
P12	184104	0	-8	-37	-86	-144	-287	-414	-528	-638	-677	-731	-805
P13	198093	0	-5	-16	-64	-121	-229	-358	-506	-598	-659	-719	-777
P14	213869	0	-4	-15	-43	-113	-197	-339	-452	-528	-558	-613	-655
P15	230534	0	-2	-6	-14	-53	-94	-207	-336	-458	-535	-598	-644
P16	247846	0	-1	-2	-9	-27	-70	-147	-216	-316	-385	-432	-471
P17	262833	0	0	-1	-2	-15	-38	-95	-155	-233	-278	-302	-359
P18	280490	0	-2	-3	-4	-12	-24	-49	-79	-107	-132	-158	-173
P19	294822	0	-1	-2	-4	-5	-11	-22	-27	-45	-53	-59	-64
P20	312943	0	0	0	-2	-3	-4	-5	-4	-6	-8	-12	-18

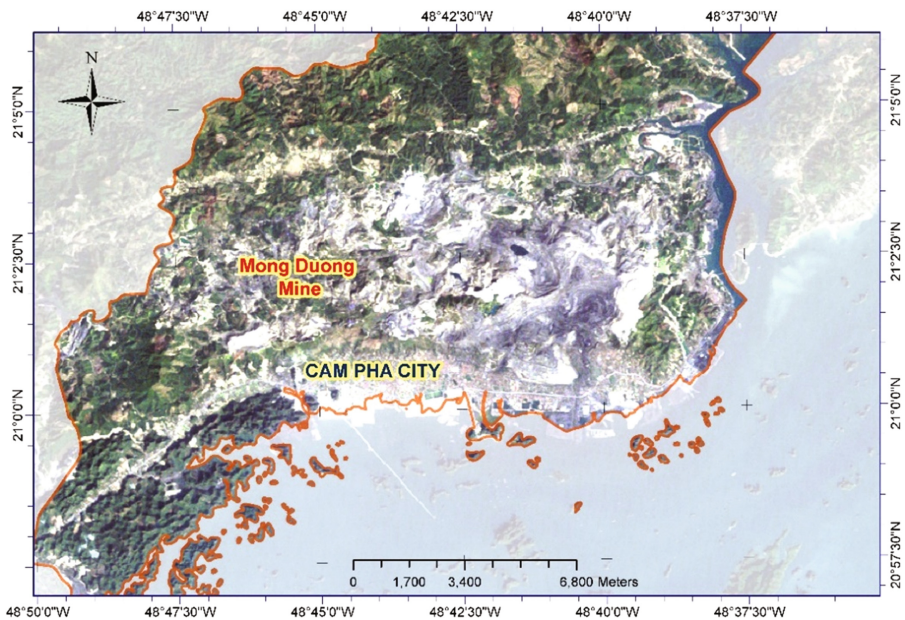**Fig. 3.** Illustration of Graphic User Interface of computational tool

Fig. 4. Mong Dong colliery location

The measurements were carried out using Leica NAK2 automatic level instrument shown in Fig. 6. The observation network consists of 2 leveling lines - the line P was established in the strike direction and the line D is along the dip direction of the Face

Fig. 5. Face No.2 with hydraulic props (photo courtesy of Long Quoc Nguyen)

Fig. 6. Leica NAK2 level

No.2, as illustrated in Fig. 7. The land subsidence data have been continuously measured from 2013 to 2015 with 12 repeated epochs. The time interval between two successive epochs is approximately 2 months. Measurement precision satisfied the Vietnam National Specifications on Mine Surveying (closed loop misclosure is less than $20\sqrt{L}$(mm) [22] with L is the total length of the leveling route.
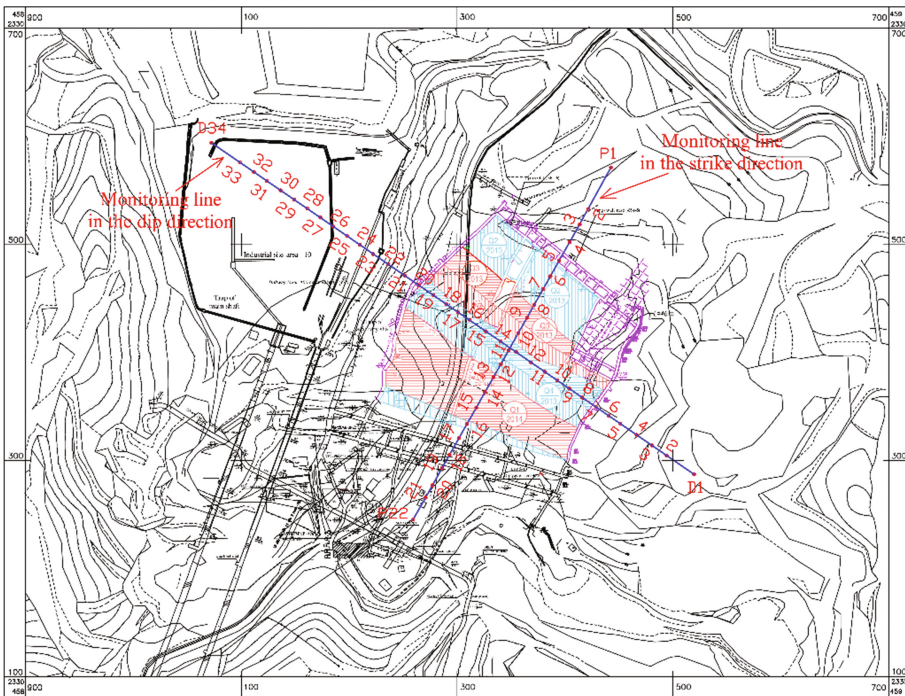

Fig. 7. The monitoring lines at the G9 BMD seam of the Mong Duong colliery

In order to detect and eliminate outliers, the difference in level between two adjacent benchmarks is determined from both forward and backward measurements. The difference in level between benchmarks is then taken equal to the average of the two values.

The monitoring observation results obtained from 16 benchmarks on the line P (see Fig. 7) were considered in the evaluation of the suitability of the algorithm used for determining the model parameters as well as the prediction accuracy of the modified KTF model. The datasets are summarized in Table 1.

Table 1. Measured subsidence (mm) with time from 16 benchmarks on line P

Point name	Cycle											
	1	2	3	4	5	6	7	8	9	10	11	12
P3	0	−1	−2	−3	−5	−9	−12	−14	−15	−17	−18	−18
P4	0	−2	−6	−11	−18	−26	−30	−35	−37	−40	−42	−43
P5	0	−7	−12	−21	−38	−55	−63	−71	−89	−96	−105	−111
P6	0	−23	−67	−85	−123	−153	−178	−195	−213	−235	−256	−279
P7	0	−17	−52	−108	−192	−258	−345	−412	−472	−541	−578	−610
P8	0	−22	−62	−129	−198	−278	−369	−452	−516	−589	−637	−664
P9	0	−25	−67	−115	−192	−342	−429	−558	−638	−725	−761	−797
P10	0	−24	−77	−102	−183	−317	−416	−547	−617	−694	−740	−783
P11	0	−15	−54	−109	−165	−303	−441	−569	−639	−711	−762	−814
P12	0	−8	−37	−86	−144	−287	−414	−528	−638	−677	−731	−805
P13	0	−5	−16	−64	−121	−229	−358	−506	−598	−659	−719	−777
P14	0	−4	−15	−43	−113	−197	−339	−452	−528	−558	−613	−655
P15	0	−2	−6	−14	−53	−94	−207	−336	−458	−535	−598	−644
P16	0	−1	−2	−9	−27	−70	−147	−216	−316	−385	−432	−471
P17	0	0	−1	−2	−15	−38	−95	−155	−233	−278	−302	−359
P18	0	−2	−3	−4	−12	−24	−49	−79	−107	−132	−158	−173

4.3   Land Subsidence Model and Its Performance Assessment

The data in the first nine cycles of 16 points were used to calibrate the subsidence model, whereas the remaining data (i.e. the data of cycles 10, 11 and 12) were used for validating the model as well as confirming its predictive capability. The algorithm described in Sect. 2 was applied to determine the parameters of the subsidence model for each point for the first 9 cycles. The calculated parameters are given in Fig. 8. The results show that the model performs well with the determining parameters set.

In this study, the authors did not use observation points such as points 1, point 2, point 19, and point 20 either to build the prediction model or to evaluate prediction results. As those points lying at the beginning and at the ending of monitoring lines, their settlement rules are not stable, hence, their subsidence curves do not match the curve for the modified KTF model.

To validate the predictive ability of the model, these calculated parameters have been used to predict the subsidence of points at the remaining cycles, i.e., the 10th, 11th and 12th cycles. The subsidence calculated from the model was subsequently compared

	Input data	Model's Parameters		Result of Prediction		Accuracy Assesment		
	Point name	ηmax	b	c	RMSE (mm)	MAE (mm)	r
1	P3	-16,378	2,648	2,604	0	0	0,997
2	P4	-40,305	2,572	2,067	1	0	0,999
3	P5	-134,787	1,030	1,673	3	2	0,996
4	P6	-281,385	1,421	1,297	4	3	0,999
5	P7	-624,896	1,409	2,003	4	3	1,000
6	P8	-822,095	1,000	1,833	4	3	1,000
7	P9	-1031,594	1,022	2,145	12	10	0,999
8	P10	-867,376	1,279	2,269	15	13	0,998
9	P11	-776,726	1,796	2,694	14	11	0,998
10	P12	-722,038	1,945	2,917	9	6	0,999
11	P13	-730,788	1,739	3,219	6	5	1,000
12	P14	-586,518	2,337	3,545	5	4	1,000
13	P15	-601,833	1,437	4,298	5	4	0,999
14	P16	-476,517	1,077	4,000	4	3	0,999
15	P17	-326,077	1,246	4,713	3	2	1,000
16	P18	-144,227	1,361	4,129	1	1	1,000
▶▶ 17							

Fig. 8. Model parameters and its accuracy

with that of observations with a deviation between predicted and monitoring data calculated by Eq. 22.

$$\Delta_i = \eta_i - \eta_i' \qquad (22)$$

where Δ_i is the difference between predicted value and its respective measurement of the ith point; η_i is the subsidence calculated from measurement data and η_i' is the value of prediction.

Small deviations shown in (Fig. 9) confirm a good model obtained. The biggest errors in prediction is at the point P9 with predicted errors at epochs 10, 11, 12 are

	Input data	Model's Parameters	Result of Prediction		Accuracy Assesment							
	Point name	Cycle 18 (η18)	Cycle 18 (η'18)	Δ18	Cycle 20 (η20)	Cycle 20 (η'20)	Δ20	Cycle 22 (η22)	Cycle 22 (η'22)	Δ22
1	P3	-16	-17	1	-16	-18	2	-16	-18	2
2	P4	-39	-40	1	-40	-42	2	-40	-43	3
3	P5	-96	-96	0	-105	-105	0	-111	-111	0
4	P6	-228	-235	7	-239	-256	17	-249	-279	30
5	P7	-520	-541	21	-556	-578	22	-581	-610	29
6	P8	-584	-589	5	-640	-637	-3	-685	-664	-21
7	P9	-755	-725	-30	-833	-761	-72	-895	-797	-98
8	P10	-704	-694	-10	-763	-740	-23	-805	-783	-22
9	P11	-711	-711	0	-747	-762	15	-765	-814	49
10	P12	-676	-677	1	-705	-731	26	-717	-805	88
11	P13	-673	-659	-14	-710	-719	9	-725	-777	52
12	P14	-570	-558	-12	-583	-613	30	-586	-655	69
13	P15	-546	-535	-11	-588	-598	10	-600	-644	44
14	P16	-392	-385	-7	-442	-432	-10	-466	-471	5
15	P17	-289	-278	-11	-317	-302	-15	-325	-359	34
16	P18	-128	-132	4	-140	-158	18	-143	-173	30
▶▶ 17										

Fig. 9. Differences between measured and predicted values

	Input data	Model's Parameters	Result of Prediction	Accuracy Assesment		
	Point name	RMSE (mm)	MAE (mm)	RMSE/Smax (%)	MAE/Smax (%)	r
1	P3	2	1	9	9	0,969
2	P4	2	2	6	5	1,000
3	P5	0	0	0	0	0,998
4	P6	21	18	7	6	0,996
5	P7	24	24	4	4	0,998
6	P8	13	9	2	1	0,994
7	P9	73	67	7	6	0,998
8	P10	20	19	2	2	0,997
9	P11	29	21	4	3	0,980
10	P12	53	39	7	5	0,948
11	P13	32	25	4	3	0,973
12	P14	44	37	7	6	0,962
13	P15	27	22	4	4	0,977
14	P16	7	7	2	1	0,989
15	P17	22	20	7	6	0,857
16	P18	20	17	14	12	0,993
17						

Fig. 10. Assessment of predicted results
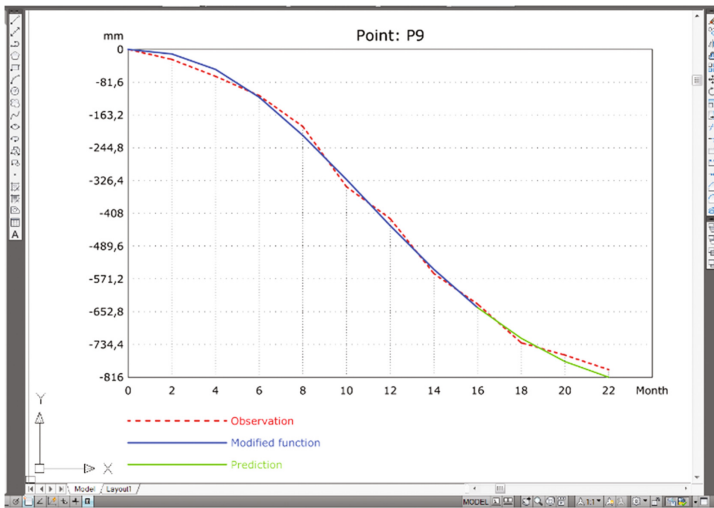
Fig. 11. Comparison of prediction and observation curves of point P9

−30 mm, −72 mm and -98 mm, respectively. These errors correspond to 4%, 8.6%, 11% of the actual subsidence magnitude of the corresponding measurement epochs. These errors are proportional to the temporal separation between the time of prediction and that of the last stage used for building prediction model, i.e., the 9th epoch. More strictly, the longer the temporal separation is, the higher error in prediction we get.

Statistical indicators including *RMSE*, *MAE*, *RMSE*$/\eta_{max}$, *MAE*$/\eta_{max}$ and *r* were used to assess the accuracy of the modified KTF model in predicting subsidence
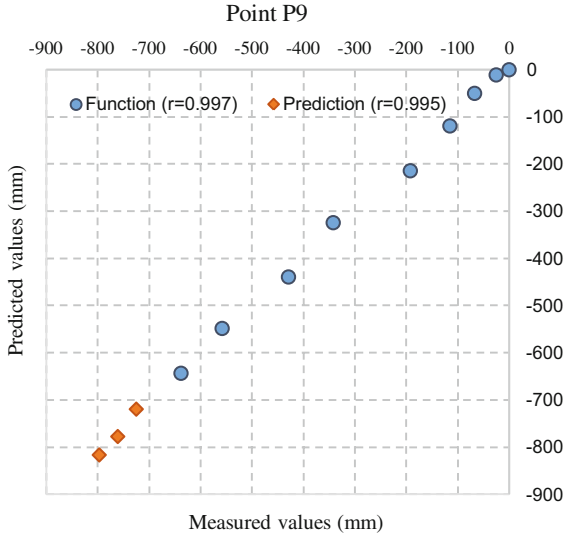
Fig. 12. Correlation between the measured and predicted values of point P9

monitored along the considered line P. The validation dataset is given in Fig. 10. It can be seen from the calculated results that the largest *RMSE* and *MAE* values are 44 mm and 37 mm, respectively, which are actually equivalent to 7% and 6% of maximum subsidence. The largest RMS/η_{max} and RMS/η_{max} values are obtained at point P18, which equal to 14% and 12%, respectively. This can be explained by the fact that this point is close to the trough subsidence edge so that the rule of point settlement has not been well-defined.

Figure 11 plots a comparison of the anticipated curve of point P9, which is calculated from Eq. (3), with the curve of actual values. It is seen from the figure that the model is able to predict very well the surface subsidence curve observed in the Mong Duong colliery.

The correlation coefficients between predicted and measured values for both cases of parameters determination and subsidence prediction are plotted in Fig. 12. With high values in the building model and the prediction results, it indicates that the predictive model is consistent with the measured data.

5 Conclusion

This research proposes a new method for calculating the preliminary values of the input parameters of the modified KTF model proposed by Chinh [19]. The method is basically based on the least-squares principle and observation data, which results in a more practical facilitation to the determination of model parameters. The computational tool has been developed incorporating a friendly user-interface and more flexibility for post-processing of the calculated results.

The functionality and accuracy of the tool were evaluated and validated against the measured subsidence values at 16 monitoring points along the observation line P which is located in the Face. No.2 at the Mong Duong colliery. The comparison result shows a very well agreement between the model prediction values and their corresponding geodetic monitoring data, where the largest *RMSE* and *MAE* are 44 mm and 37 mm, respectively. The smallest correlation coefficient r is calculated equal to 0.857, which indicates a high correlation between the monitoring measurements and their predicted values. It is concluded that the developed tool incorporating the modified KTF model is useful and suitable for predicting and evaluating potential mining-induced subsidence in the mining industry. Thereby, the tool can support appropriate strategy to prevent and minimize potential impact caused by land subsidence phenomenon.

A main limitation of this research work is that points lying at the beginning and at the end of the observation line have been excluded from the calculation model as they could have influenced by an irregular process of subsidence. The modified KTF applied in this research, therefore, cannot represent the subsidence of these points over time. More flexible prediction models are thus necessary.

Conflict of interest. The authors declare that there is no conflict of interest.

References

1. Reddish, D., Whittaker, B.: Subsidence: Occurrence. Prediction and Control. Elsevier, New York (1989)
2. Can, E., Kuşcu, Ş., Kartal, M.E.: Effects of mining subsidence on masonry buildings in Zonguldak hard coal region in Turkey. Environ. Earth Sci. **66**, 2503–2518 (2012)
3. Bozeman, M.: Underground Hard-Rock Mining: Subsidence and Hydrologic Environmental Impacts. Google Scholar (2002)
4. Phung, D.M.: Selection of Appropriate Technical and Technological Solutions for Exploitation in Areas Where Existing Historical, Cultural, Industrial and Civil Works. Vinacomin (2011)
5. Truc, K.K.: Defining land subsidence parameters of Thongnhat coal mine. Institute of Mining Science and Technology (1991)
6. Long, Q.N.: Sectional diagram of dynamic subsidence trough at the Mong Duong coal mine: evaluation and prediction. J. Min. Earth Sci. (JMES) **56**, 58–66 (2016)
7. Long, Q.N., My, C.V., Luyen, K.B.: Divergency verification of predicted values and monitored deformation indicators in specific condition of Thong Nhat underground coal mine (Vietnam). Geoinf. Pol. **15**, 15–22 (2016)
8. Jarosz, A., Karmis, M., Sroka, A.: Subsidence development with time—experiences from longwall operations in the appalachian coalfield. Geotech. Geol. Eng. **8**, 261–273 (1990)
9. Liu, X., Wang, J., Guo, J., Yuan, H., Li, P.: Time function of surface subsidence based on Harris model in mined-out area. Int. J. Min. Sci. Technol. **23**, 245–248 (2013)
10. Bahuguna, P., Srivastava, A., Saxena, N.: A critical review of mine subsidence prediction methods. Min. Sci. Technol. **13**, 369–382 (1991)

11. Hu, Q.F., Cui, X.M., Wang, G., Wang, M.R., Ji, Y.X., Xue, W.: Key technology of predicting dynamic surface subsidence based on knothe time function. JSW **6**, 1273–1280 (2011)
12. Zhang, Z., Zou, Y., Chen, J., Wang, Y.: Prediction model of land dynamic settlement in coal mining subsidence area. Trans. Chin. Soc. Agric. Eng. **32**, 246–251 (2016)
13. Lian, X.: Prediction model of dynamic subsidence caused by underground coal mining. Electron. J. Geotech. Eng. **21** (2016)
14. Hu, Q., Deng, X., Feng, R., Li, C., Wang, X., Jiang, T.: Model for calculating the parameter of the Knothe time function based on angle of full subsidence. Int. J. Rock Mech. Min. Sci., 19–26 (2015)
15. Wang, C.: Analysis on the improved time function model of surface subsidence. Electron. J. Geotech. Eng. **19** (2015)
16. Zhanqiang, C., Jinzhuang, W.: Study on the time function of surface subsidence - The Improved Knothe time function. Chin. J. Rock Mechan. Eng. **9**, 018 (2003)
17. Cui, X., Miao, X., Wang, J.A., Yang, S., Liu, H., Song, Y., Liu, H., Hu, X.: Improved prediction of differential subsidence caused by underground mining. Int. J. Rock Mech. Min. Sci. **37**, 615–627 (2000)
18. Han, H.L., Cui, B.: Modeling of surface subsidence based on time function. Adv. Mater. Res. **422**, 318–321 (2012)
19. Chinh, N.D.: Geodetic Methods for Geodynamics. Hanoi University of Mining and Geology, Hanoi (2003)
20. https://www.devexpress.com/
21. https://www.autodesk.com/techpubs/autocad/acadr14/dxf/dxf_reference.htm
22. Ministry of Information & Communications: Vietnam National Specifications on Mine Surveying, Vietnam (2015)